ACS APPLIED MATERIALS & INTERFACES

Research Article

www.acsami.org

Rigid–Flexible Coupling High Ionic Conductivity Polymer Electrolyte for an Enhanced Performance of $LiMn_2O_4$/Graphite Battery at Elevated Temperature

Pu Hu,[†,‡] Yulong Duan,[†] Deping Hu,[†,‡] Bingsheng Qin,[†] Jianjun Zhang,[†] Qingfu Wang,[†] Zhihong Liu,[†] Guanglei Cui,*[,†] and Liquan Chen[§]

[†]Qingdao Industrial Energy Storage Research Institute, Qingdao Institute of Bioenergy and Bioprocess Technology, Chinese Academy of Sciences, Qingdao 266101, People's Republic of China

[‡]University of Chinese Academy of Sciences, Beijing 100049, People's Republic of China

[§]Beijing National Laboratory for Condensed Matter Physics, Institute of Physics, Chinese Academy of Sciences, Beijing 100190, People's Republic of China

Supporting Information

ABSTRACT: $LiMn_2O_4$-based batteries exhibit severe capacity fading during cycling or storage in $LiPF_6$-based liquid electrolytes, especially at elevated temperatures. Herein, a novel rigid–flexible gel polymer electrolyte is introduced to enhance the cyclability of $LiMn_2O_4$/graphite battery at elevated temperature. The polymer electrolyte consists of a robust natural cellulose skeletal incorporated with soft segment poly(ethyl α-cyanoacrylate). The introduction of the cellulose effectively overcomes the drawback of poor mechanical integrity of the gel polymer electrolyte. Density functional theory (DFT) calculation demonstrates that the poly(ethyl α-cyanoacrylate) matrices effectively dissociate the lithium salt to facilitate ionic transport and thus has a higher ionic conductivity at room temperature. Ionic conductivity of the gel polymer electrolyte is 3.3×10^{-3} S cm^{-1} at room temperature. The gel polymer electrolyte remarkably improves the cycling performance of $LiMn_2O_4$-based batteries, especially at elevated temperatures. The capacity retention after the 100th cycle is 82% at 55 °C, which is much higher than that of liquid electrolyte (1 M $LiPF_6$ in carbonate solvents). The polymer electrolyte can significantly suppress the dissolution of Mn^{2+} from surface of $LiMn_2O_4$ because of strong interaction energy of Mn^{2+} with PECA, which was investigated by DFT calculation.

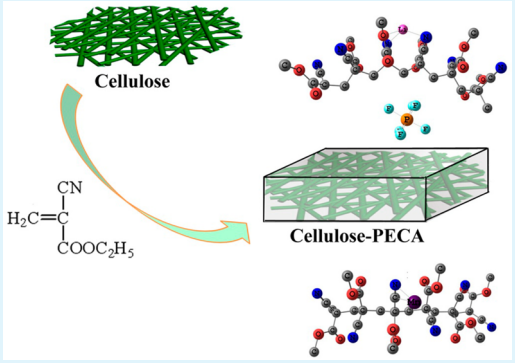

KEYWORDS: *Li-ion battery, polymer electrolyte, poly(ethyl α-cyanoacrylate), $LiMn_2O_4$*

INTRODUCTION

Lithium ion batteries (LIBs) have been widely used as power sources for portable devices due to their high energy density, long cycle life, and minimal memory effects. Large-capacity LIBs are also promising power sources for electric vehicles and large-scale energy storage systems. Improved safety combined with longer cycle life is very crucial for large-scale LIB applications. Compared to other commercial cathode materials (layered $LiCoO_2$, $LiNiO_2$, $LiNi_xMn_yCo_{1-x-y}O_2$), spinel $LiMn_2O_4$ is one of the most promising cathode materials for large-formate LIB applications because of their special 3D tunnel crystalline structure and excellent electrochemical performance.[3,4] However, $LiMn_2O_4$-based batteries exhibit severe capacity fading during cycling or storage in the $LiPF_6$-based liquid electrolytes, especially at elevated temperatures, resulting from manganese (Mn^{2+}) dissolution and interfacial side reaction between the electrolyte and the surface of the electrode.[5,6] In a typical $LiMn_2O_4$/graphite (LMO/G) full-cell, the dissolved manganese is reduced to metallic Mn and subsequently catalyzes the decomposition of electrolyte, which degenerates the solid electrolyte interface (SEI) layer formed on anode surface.[7,8] Thus, a dramatic capacity fading often occurs in LMO/G batteries, especially at elevated temperature, where the Mn^{2+} dissolution and interfacial side reaction become amplified. To date, several kinds of strategies, such as cationic doping and/or surface coating of $LiMn_2O_4$, functional additives in the electrolyte,[1] and surface modification[10,11] have been taken to improve cycling ability of $LiMn_2O_4$-based batteries. However, the long-term stable battery of LMO/G is still one of the main challenges for the practical application.

Compared with liquid electrolytes, the safety and stability of batteries can be significantly improved in systems using polymer electrolyte because of their good electrochemical and thermal stability. Gel polymer electrolyte (GPE) is regarded as

Received: November 29, 2014
Accepted: February 5, 2015
Published: February 5, 2015

DOI: 10.1021/am5083683
ACS Appl. Mater. Interfaces 2015, 7, 4720–4727

an effective solution to the above-mentioned issues of $LiMn_2O_4$-based batteries by suppressing the Mn^{2+} dissolution and interfacial side reaction between the electrode and electrolyte.[12,13] In our previous study,[14,15] a class of single-ion GPE that exhibits good thermal stability and high ionic conductivity was explored for improving cycle performance of $LiMn_2O_4$/Li batteries at elevated temperatures. Recently, efforts have been devoted to explore several matrix of polymer electrolytes, including poly(ethylene oxide)[16] (PEO), poly(vinylidene fluoride)[17] (PVDF), poly(acrylonitrile)[18] (PAN), poly(vinyl chloride),[19] and poly(methyl methacrylate).[20] However, from a practical point of view, ionic conductivity and mechanical properties of most of those polymer matrix materials cannot fully match the requirements of LIBs.

In the present study, a rigid−flexible coupling composite membrane that exhibits high ionic conductivity and excellent mechanical property was developed as a polymer electrolyte to achieve better cyclability of LMO/G batteries. The composite membrane, based on a soft segment poly(ethyl α-cyanoacrylate) (PECA) and a robust natural cellulose skeleton, was prepared using an in situ polymerization method. The in situ polymerization is beneficial for the interfacial contact between PECA and cellulose, which contributes to high ionic conductivity as well as favorable mechanical properties and interfacial compatibility of electrodes. The obtained GPE exhibits good interfacial stability between electrode and electrolyte, thus improving the overall electrochemical performance of $LiMn_2O_4$-based batteries, especially at elevated temperatures.

EXPERIMENTAL SECTION

Ethyl α-cyanoacrylate was first diluted by anhydrous acetone (volume ratio: 1/3) to obtain a transparent solution. Then the cellulose membrane was fixed on a polytetrafluoroethylene (PTFE) plate, and the ethyl α-cyanoacrylate solution was cast-coated. The composite membrane could be prepared due to rapid polymerization of ethyl α-cyanoacrylate in the cellulose skeleton in air. After drying, the obtained composite membranes (d = 1.65cm) were saturated in a common electrolyte (1 M $LiPF_6$ solution in EC/DMC, 1/1, w/w,) in an argon-filled glovebox to obtain the GPEs.

The $LiMn_2O_4$ electrode was made by mixing 90 wt % $LiMn_2O_4$, 5 wt % PVDF, and 5 wt % carbon black onto an Al current collector. The anode electrode was made by mixing graphite/Super-p/CMC (carboxymethyl cellulose)/SBR (styrene butadiene rubber) with the mass ratio of 95.5/1.0/1.5/2.0). All cells were assembled in an argon-filled glovebox. The charge/discharge behavior of cells were tested on a LAND battery test system at the potential range of 3.0−4.3 V.

The AC impedance was analyzed over a frequency range of 0.1−10^6 Hz with a perturbation amplitude by a Zahner Zennium electrochemical working station of 5 mV. The variation in electrode polarization during cycling was measured using cyclic voltammetry (CV). The surface morphology of the graphite anode and the $LiMn_2O_4$ cathodes after 100 cycles was observed by field emission scanning electron microscopy (FE-SEM, Hitachi S-4800). The element compositions were examined by energy dispersive X-ray spectroscopy (EDX, HoRiBA 7593-H) at a magnification of 5000× and an accelerating voltage of 15.0 kV.

COMPUTATION METHODS

All the calculations were implemented at the B3LYP/6-31G* level with the Gaussian 09 program. The hexameroligomer was chosen as the model to mimic the polymer. The structure of the oligomer was first optimized. Then we added the ions and optimized the whole system with constraining the skeleton of the oligomer. At the optimized structures, the frequency calculations were used to predict the Raman spectrum. The density functional theory (DFT) method could cause overestimation of the fundamental modes; therefore, a scaling factor (0.9614) was used in order to get a better match of the experimental data.

RESULTS AND DISCUSSION

In the ethyl α-cyanoacrylate molecules, two electron withdrawing groups, cyan group and ester group, are linked to the same carbon atom, which makes them easy for polymerization. The polymerization reaction could be easily initiated even if there is a trace amount of weak bases, such as water, but chain termination only happens when there is some strong acid. Therefore, a rigid−flexible coupling composite membrane could be simply and rapidly obtained by in situ polymerization, when a robust natural cellulose membrane as a skeleton was soaked into the ethyl α-cyanoacrylate monomer.

To visualize the structure of the polymer matrix in GPEs, SEM images of the surface and cross section of cellulose and composite membrane were collected. An obviously porous network of pristine cellulose membrane was observed, as shown in Figure 1a. The pore shape of the pristine cellulose membrane

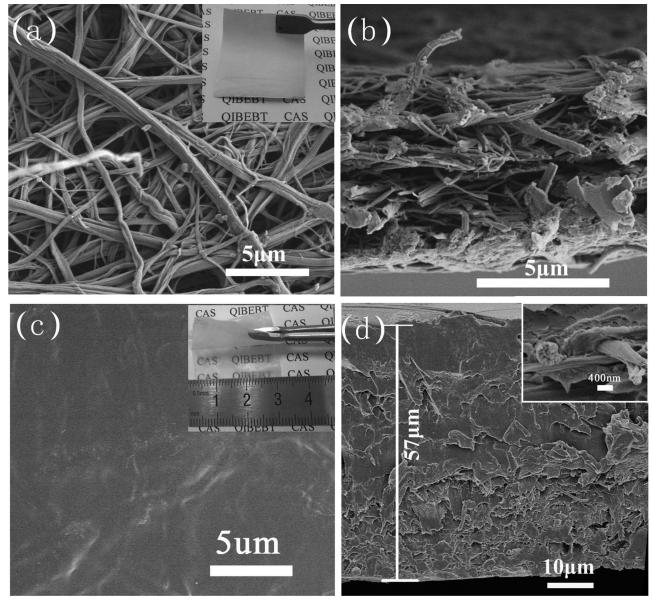

Figure 1. Typical SEM images of surface (a) (inset shows the photograph of cellulose membrane) and cross section (b) of cellulose membrane; SEM images of surface (c) (inset shows the photograph of composite membrane), and cross section (d) of composite membrane (inset shows the magnified patterns).

is irregular, and the size distribution is unequal (about 1−5 μm). This pore size is much larger than that of commercial separators. Generally speaking, cellulose matrix with large pore size is not favorable to be used as separators of LIBs directly. So here after compositing with PECA by in situ polymerization, the pores of the cellulose were covered with PECA polymer, thus a dense and uniform layer was formed on the surface of the membrane (Figure 1c). Inset of Figure 1c shows the photograph of the PECA−cellulose composite membrane, which is flexible and transparent. From the cross section of the micrographs (Figure 1d), the inner space of the cellulose skeleton was also filled with the polymer matrix. The thickness of the composite membrane is about 57 μm, which is slightly

DOI: 10.1021/am5083683
ACS Appl. Mater. Interfaces 2015, 7, 4720−4727

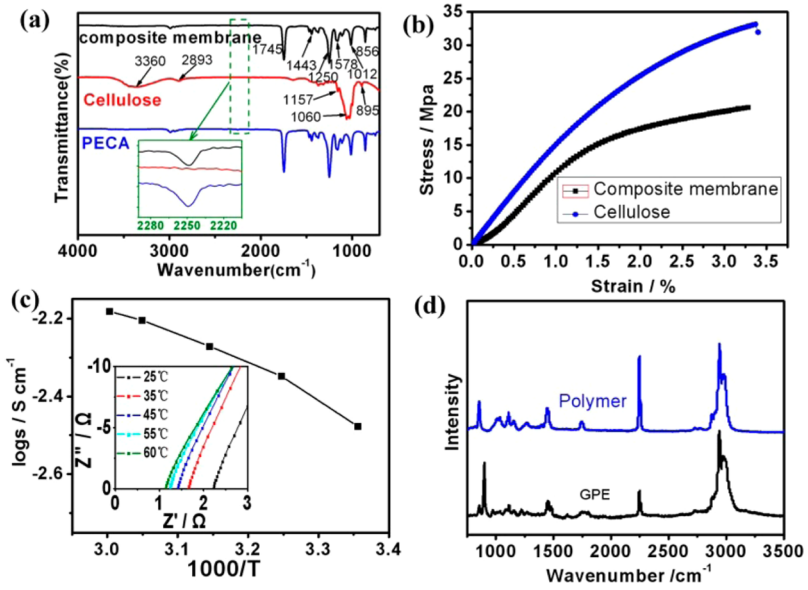

Figure 2. (a) IR spectra of composite membrane, cellulose and PECA (inset shows the magnified patterns); (b) stress−strain curves of composite membrane and cellulose; (c) ionic conductivities of the GPE at different temperatures (inset is the Nyquist impedance data); (d) Raman spectra of the PECA and the GPE.

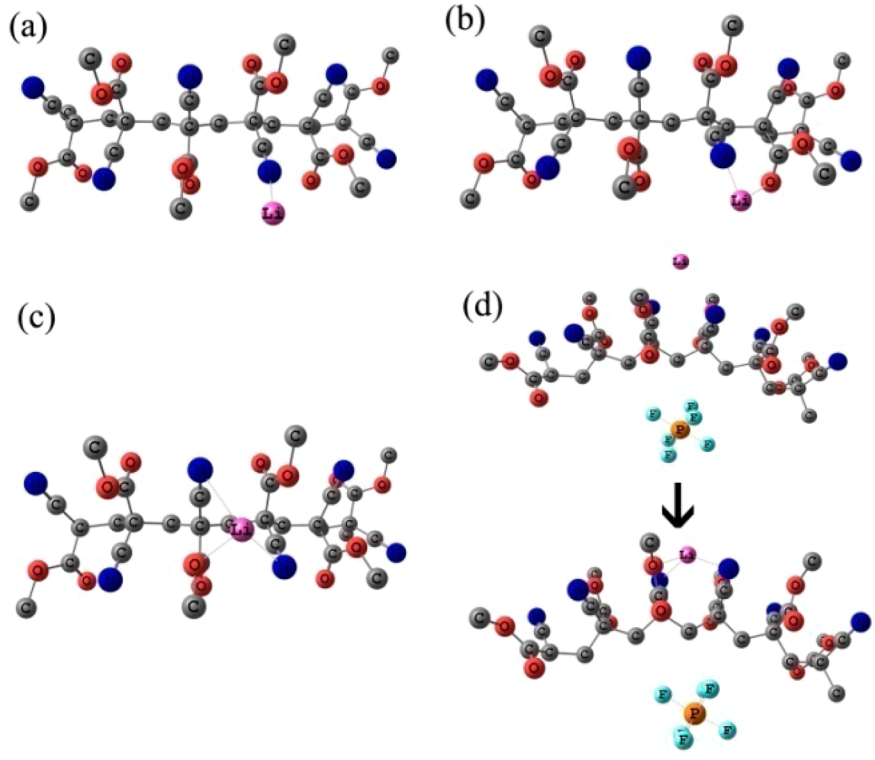

Figure 3. Schematic illustration of main interaction forms between the Li^+ and the polymer in the GPE. (a) Li^+ contacts with one N atom only (denoted as I); (b) Li^+ contacts with one N atom and one O atom (denoted as II); (c) Li^+ contacts with two N atoms and one O atom (denoted as III); the corresponding binding energy of these three forms are 1.60, 1.97, and 1.86 kcal/mol, respectively. (d) One Li^+ and one PF_6^- were put on both sides of the polymer, respectively (up), and then the optimized structure (down) was obtained.

thicker than that of pristine cellulose membrane. Figure 2a compares the IR spectra of pristine cellulose, PECA, and the PECA−cellulose composite. The red line in Figure 2a shows the spectra of pristine cellulose. The position around 3360, 1060, and 895 cm^{-1} are attributed to −O—H stretching, −C—O stretching, and cyclic C—O—C asymmetric stretching vibration. In the PECA−cellulose composite membrane, peaks at about 3000−2800 cm^{-1} (C—H stretching in $-CH_2$ and $-CH_3$), 2249 cm^{-1} (−CN stretching), 1745 cm^{-1} (−C═O stretching), and 1250 cm^{-1} (C—O—C symmetric) could be attributed to the absorption peaks of PECA. The spectra of the PECA−cellulose composite membrane contain all the peaks of cellulose and PECA, indicating the composite membrane is successfully prepared.

DOI: 10.1021/am5083683
ACS Appl. Mater. Interfaces 2015, 7, 4720−4727

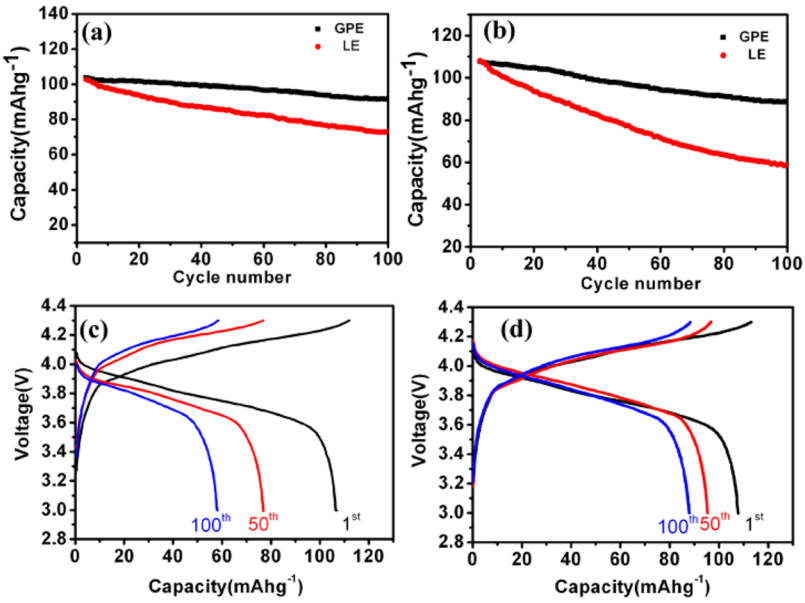

Figure 4. Cycle performance of LMO/G full battery at ambient temperature (a) and high temperature of 55 °C (b); charge−discharge curves of batteries cycling in liquid electrolyte (c) and GPE (d) at 55 °C.

As is well-known, commercially available GPE has some limitations for the further application in LIBs because its mechanical property is generally poor. Natural cellulose, the important structural component in green plants, is the most abundant raw material in nature. Cellulose-based nonwoven fabrics, as the skeletal component in GPE, could serve as a free-standing thin film to avoid the tedious processing for gel polymer electrolyte, and increase mechanical properties enough for large-scale applications. As depicted in Figure 2, the maximum stress of the composite membrane reached 33 MPa, much higher than that of the cellulose separator (20 MPa), which indicates the enhancement of mechanical strength by a synergetic effect of the cellulose skeletal and compositing polymer. The tensile strength of composite membrane was definitely higher than the transverse strength of the commercial PP separator (14 MPa) and lower than that of PP separator at the machine direction (120 MPa),[21] as the obtained mechanical strength is acceptable for polymer electrolyte to remain mechanical integrity and prevent the membrane falling apart in Li-ion battery system. Interestingly, the composite membrane presents a substantially higher Young's modulus (1640 MPa), which is much higher than the value of commonly used PP membrane (240 MPa).The enhancement of mechanical property is attributed to its integrated structure in which porous network cellulose acts as an efficient skeletal component filled entirely with polymer in its space.

Normally, polymer electrolytes need to reach a high ionic conductivity (10^{-2}−10^{-3} S cm^{-1}) to ensure low Ohmic drops. As shown in Figure 2c, the ionic conductivity of the GPE based on PECA−cellulose membranes reaches 3.3×10^{-3} S cm^{-1} at ambient temperature, which is comparable to the commercial liquid electrolyte in previous reports.[21,22] It is known that the high ionic conductivity results from the dissociation of salt in the host polymer matrix and ion mobility. Both ester and cyan groups with strong electron withdrawing capability on the side chains of PECA can favorably facilitates the dissociate of the electrolytic salt, leading to a enhanced ionic conductivity of GPE. Theory calculation illustrates that the Li^+ can interact with the polymer in the GPE in three forms, as shown in Figure 3, the strong interaction with N in cyano group, and with O in the ester group. Figure 2d shows the Raman spectroscopy of the PECA and the GPE electrolyte. It is clearly shown that the intensities of the peaks of PECA at 2246, 1700, and 1100 cm^{-1}, which belongs to the C≡N stretching vibration, free carbonylis, and the C—O—C stretching vibration, are slower than that in GPE, indicating the strong interaction between Li^+ and the group in GPE. These results are well in agreement with the theoretical calculation Raman spectroscopy (Figure S2, Supporting Information). It can be clearly seen that cyano group stretching vibration is greatly reduced in experimental spectra because three interactions that form (I, II, and III in Figure 3) between polymer and Li^+ are related to the N atom in the cyano group. These binding sites interacting with Li^+ in polymer are beneficial to the separation of ion pairs in electrolyte and thus increase the dissociation of the electrolytic lithium salt.[23] Therefore, the PECA-based GPE shows higher Li^+ conductivity, which stems from the easier dissociation of $LiPF_6$ by PECA. Because PF_6^- is a big anion group, theoretic calculation cannot obtain any optimized stable forms for PF_6^- combined with polymer. It is suggested that interacting with Li^+ and/or the anion in polymer is beneficial to the separation of ion pairs in electrolyte and thus increases the dissociation of the electrolytic lithium salt. Figure 3d illustrates that cyano and ester groups can separate the Li^+ and anions on two sides of the polymer because of the strong interaction and steric hindrance, which prevent the reconnection between Li^+ and anions, thus rendering the GPE a higher ionic conductivity.

To investigate the GPE influence on the cycling performance of the batteries at ambient conditions and elevated temperature, full-cells (LMO/G) were tested at a charge/discharge rate of 0.5C in the potential range of 3.0−4.3 V. At ambient temperature, the cycling performance of the battery employing GPE was slightly improved compared to that of conventional liquid electrolyte (Figure 4a). The GPE cell maintained 90% of the initial discharge capacity after 100 cycles, while the cell-based liquid electrolyte retained a lower portion of 71% (73 mAh g^{-1}) of the initial discharge capacity after the same cycles. However, the difference of capacity retention of the two cells

DOI: 10.1021/am5083683
ACS Appl. Mater. Interfaces 2015, 7, 4720−4727

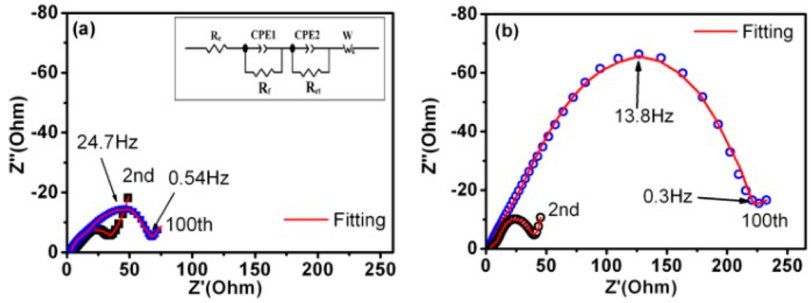

Figure 5. EIS of batteries at the charged state after 2 and100 cycles: (a) GPE (inset shows equivalent circuit) and (b) liquid electrolyte.

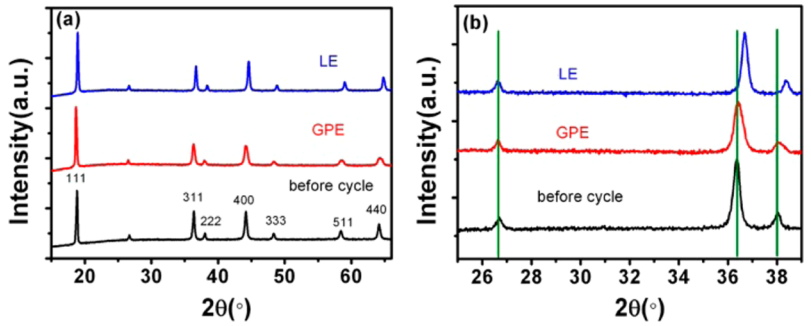

Figure 6. (a) XRD patterns of the $LiMn_2O_4$ electrodes before and after 100 cycles at 55 °C in LE and GPE; (b) magnified patterns.

became more pronounced at an elevated temperature of 55 °C. As shown in Figure 4b, the capacity retention after the 100th cycle is much higher for the GPE-based battery than that of liquid electrolyte, demonstrating that the cycling performance of the battery could be significantly improved in using GPE as the electrolyte at the elevated temperature. It is obviously shown in the charge/discharge profiles (Figure 4c) that shorter plateaus and larger potential separation between charge and discharge are present in a battery of liquid electrolyte than those in GPE. GPE-based batteries exhibits little variation in potential gap with the increasing of cycling number, indicating that batteries with GPE suppress the deterioration of the polarization at higher temperature. It is generally accepted that the polarization of the batteries is caused by mass and charge transfer at the interface of electrolyte and electrodes.[22,24] Therefore, it could be deduced that gradual deterioration of interfacial layer of batteries while cycling in liquid electrolyte-based system hinders the mass and charge transfer at the interface of electrolyte and electrodes.

It is reported that the interfacial layer is growing with increasing cycling due to the unfavorable reaction at the surface of materials of cathode and anode, especially at higher temperature, which accelerates the capacity fading. To better understand the different behaviors in terms of electrochemical property and polarization with GPE and liquid electrolyte, electrochemical impedance spectroscopy (EIS) of the batteries was measured after cycling at an elevated temperature of 55 °C. The EIS spectra are compared in Figure 5. Each spectrum contains two depressed semicircles at high frequency and a sloping line in the low frequency. According to the reaction mechanism of the LMO/G battery proposed by previous studies,[25,26] the first semicircle can be ascribed to Li^+ diffusion through SEI film on the electrode (denoted as R_f), and the second semicircle is assigned to charge transfer resistance (denoted as R_{ct}), and the followed sloping line can be ascribed to Li^+ diffusion in the bulk material. To simulate the results of the obtained EIS, typical equivalent circuit (inset of Figure 5a) was used. The results of the simulation are shown in the Supporting Information. It turned out that the R_f and R_{ct} of the liquid electrolyte are 26.3 and 200.7 Ω in the 100th cycle, respectively, which are significantly higher than the values in the 2nd cycle. The results suggest that the severe capacity fading of the batteries based on liquid electrolyte could be due to the increasing of R_f and R_{ct}, which may be caused by the further deteriorative solid-electrolyte interphase (SEI) layer on the anode because of an unstable interface between the electrolyte and electrode. By contrast, although the R_e in the cell with the GPE was slightly higher than that of the liquid electrolyte, the increase of the values of both R_f (from 12.3 to 18.8 Ω) and R_{ct} (from 26.1 to 44.9 Ω) are remarkably suppressed from the 2nd to 100th cycle. This demonstrated that the GPE-based batteries may have a stable interface between electrolyte and electrode, which results in much less decomposition of the liquid electrolyte, providing better cyclability at elevated temperatures.

Figure 6 presents the XRD patterns of the $LiMn_2O_4$ electrodes before and after cycling in GPE and LE at 55 °C. All diffraction peaks of the $LiMn_2O_4$ electrodes before cycling matched well with cubic spinel except the peak at 26.6°, which is ascribed to the conductive carbon. After 100 cycles, the diffraction peaks of carbon remained; however, the peaks of $LiMn_2O_4$ shift to a higher angle after cycling in LE, as shown in the magnified patterns (Figure 6b). This results from the shrinkage of crystal lattice due to the dissolution of Mn^{3+} ions from the spinel structure during cycling at the elevated temperature.[27] And the positions of XRD peaks for LMO after cycling in GPE shift much less significantly than those of LMO cycled in LE, indicating that GPE can inhibit manganese dissolution from $LiMn_2O_4$.

Figure 7 presents the XPS spectra of F_{1s} and Mn $_{2p}$ of the $LiMn_2O_4$ cathodes after in LE and GPE at 55 °C, respectively. The F_{1s} spectra (in Figure 7a) contain two main peaks: LiF (685.0 eV) and PVdF (687.6 eV).[28] Note that the relative

DOI: 10.1021/am5083683
ACS Appl. Mater. Interfaces 2015, 7, 4720−4727

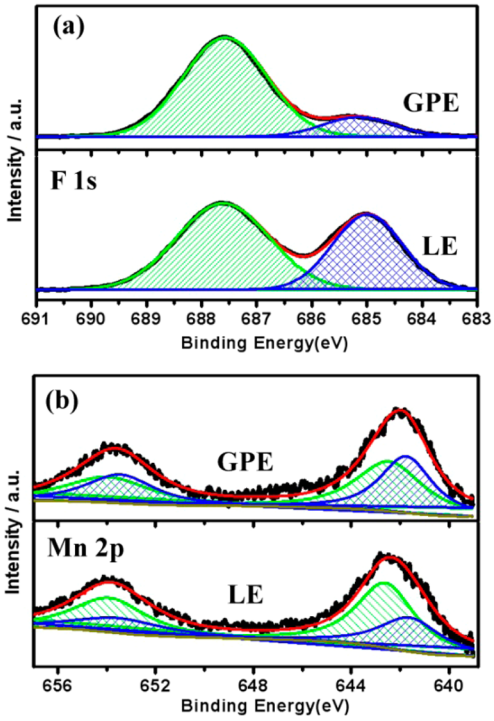

Figure 7. F 1s (a) and Mn 2p (b) XPS spectra of $LiMn_2O_4$ cathodes after 100 cycles at 55 °C in LE and GPE, respectively.

intensity of PVdF is similar after cycling in GPE and LE, while the relative intensity of LiF increased obviously after cycling in LE, indicating the decomposition products of the electrolyte in LE is more severe than GPE at the surface of the $LiMn_2O_4$ electrode. It is depicted in Figure 7b that Mn_{2p} peaks after 100 cycles of electrode materials in LE shift to a higher binding energy than that in GPE, indicating higher valence of manganese on the surface of electrode cycling in LE. Based on the position as well as the integrated area of Mn_{2p} peaks, the average oxidation state of Mn is calculated to be 3.55 and 3.45 in the surface of electrodes cycling in LE and GPE, respectively. It is well-known that Mn^{3+} of $LiMn_2O_4$ undergoes a disproportion reaction generating Mn^{4+} and soluble Mn^{2+}:[1,27,29−31]

$$2Mn^{3+}(s) \rightarrow Mn^{2+}(aq) + Mn^{4+}(s) \quad (1)$$

According to eq 1, the Mn^{2+} ions of the LMO cathode gradually dissolved into liquid electrolyte during the cycling and got a higher ratio of Mn^{4+}/Mn^{3+}. The higher average oxidation of Mn in LE than that in GPE can be ascribed to larger amount dissolution of Mn^{2+} on the surface in liquid electrolyte. Due to the metatheses reaction of Mn^{3+}, the dissolution of Mn^{2+} leads to the loss of active Mn^{3+} in LMO and thus cause the severe capacity fading.[32] It is to say that the obtained rigid−flexible coupling high ionic conductivity GPE can significantly suppress the dissolution of Mn^{2+} and benefit for the cycling performance at elevated temperatures.

To confirm the corrosion of the electrodes, SEM imaging was carried out to obtain the surface morphology of graphite anode after the battery was cycled 100 times at 55 °C. As shown in Figure 8, the SEM images of the graphite electrode cycling in GPE showed a smooth surface similar to the pristine electrode before cycling, as shown in Figure 8a. By contrast, the graphite electrode shows some deposits on the surface after cycling in liquid electrolyte, which can be regarded as the formation of SEI and deposition of manganese according to previous literature.[6,33,34] EDS detection confirms that these deposites are consisted of a relatively higher concentration of Mn element on the surface of graphite (Figure S2, Supporting Information), which demonstrates that the dissolved Mn^{2+} in electrolyte solution was deposited on the anode surface during the cycling process at high temperatures. The similar phenomenon is found in the battery electrode cycled at ambient temperature, as shown in Figure S3 (Supporting Information). However, the variation of surface morphology of the graphite anode is not clear for electrodes cycled in GPE and LE at ambient temperature, which indicated that manganese reduction is less significant than that at elevated temperatures.

It is reported that capacity fading of LMO/G batteries is not only due to the loss of active compound (Mn^{3+}) caused by the dissolution of Mn, but more often due to the fact that the migration of the dissolved Mn deposits on to the surface of the anode, which destroyed the fine structure the SEI layer.[12,32] According to Zhan's work,[35] it is found such deposites on anode are compounds of Mn^{2+}, which could have some complicated reaction with species on SEI layer. Therefore, the continuous dissolution of Mn in LMO cathode will ceaselessly damage the SEI film on the surface of graphite. It is suggested that effective prevention of the migration and deposition of dissolvedMn is critical to the performance of LMO/G battery. In the present study, theoretical calculation shown that the binding energy of Mn^{2+} with PECA is much higher than that of Li^+ (Figure S4, Supporting Information), indicating that dissolved Mn^{2+} from cathodes is hard to diffuse in GPE. Thus, contents of Mn element on the surface of the anode for a GPE-based battery is much less than that for a LE-based battery, confirming that GPE can inhibit manganese deposition. These findings demonstrated that the GPE is a very promising electrolyte candidate for the LMO/G battery to tackle their challenges of storage and cycling characteristic at the elevated temperatures.

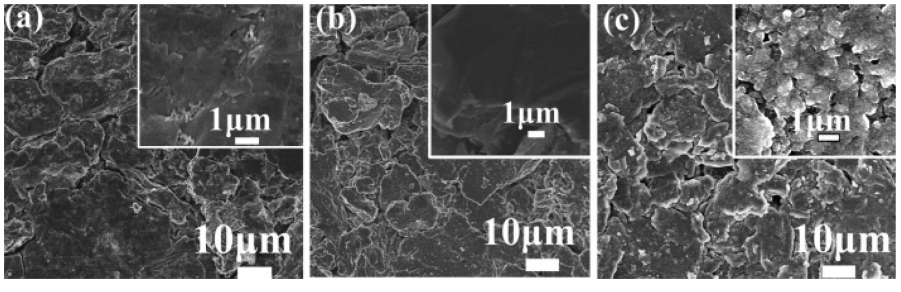

Figure 8. Typical SEM images of graphite anode before cycling (a) and after 100 cycles at 55 °C in GPE (b) and in LE (c), respectively.

DOI: 10.1021/am5083683
ACS Appl. Mater. Interfaces 2015, 7, 4720−4727

CONCLUSIONS

A rigid−flexible composite membrane based on soft segment PECA and a robust natural cellulose skeleton has been prepared by an in situ polymerization process. The composite membrane shows enhanced mechanical strength compared with that of a pure cellulose membrane. After gelation in a solution of electrolyte, it a exhibits excellent ionic conductivity (3.3×10^{-3} S cm^{-1}) at room temperature. The high conductivity could be ascribed to easier dissociation of $LiPF_6$ by PECA. The obtained GPE remarkably improves the cycling performance of $LiMn_2O_4$ electrodes compared to the conventional liquid electrolyte, especially at the elevated temperature, because of the superior interfacial stability.

ASSOCIATED CONTENT

Supporting Information

Theoretic analysis of main interaction forms between the Li^+ and the polymer in the GPE, SEM graphs and corresponding EDS spectra of electrode after 100 cycles in GPE and in LE at 55 °C, SEM graphs and corresponding EDS spectra of electrode after 100 cycles in GPE and in LE at room temperature, schematic illustration of main interaction forms between the Mn^{2+} and the polymer in the GPE, and simulation results of AC impedance spectra. This material is available free of charge via the Internet at http://pubs.acs.org.

AUTHOR INFORMATION

Corresponding Author

*G. Cui. Tel.: +86-532-80662746. E-mail: cuigl@qibebt.ac.cn.

Notes

The authors declare no competing financial interest.

ACKNOWLEDGMENTS

This work was supported by the National Basic Research Program of China (Grant No. 2011CB935700), the National Natural Science Foundation of China (No. 21344003), the Key Research Program of the Chinese Academy of Sciences (Grant No. KGZD-EW-202-2), and the Strategic Priority Research Program of the Chinese Academy of Sciences (Grant No. XDA09010105).

REFERENCES

(1) Jang, D. H.; Shin, Y. J.; Oh, S. M. Dissolution of Spinel Oxides and Capacity Losses in 4V $Li/Li_xMn_2O_4$ Cells. *J. Electrochem. Soc.* **1996**, *143*, 2204−2211.

(2) Kim, J.-S.; Kim, K.; Cho, W.; Shin, W. H.; Kanno, R.; Choi, J. W.; Truncated, A. Manganese Spinel Cathode for Excellent Power and Lifetime in Lithium-Ion Batteries. *Nano Lett.* **2012**, *12*, 6358−6365.

(3) Zhong, Q. M.; Bonakdarpour, A.; Zhang, M. J.; Gao, Y.; Dahn, J. R. Synthesis and Electrochemistry of $LiNi_xMn_{2-x}O_4$. *J. Electrochem. Soc.* **1997**, *144* (1), 205−213.

(4) Kim, D. K.; Muralidharan, P.; Lee, H.-W.; Ruffo, R.; Yang, Y.; Chan, C. K.; Peng, H.; Huggins, R. A.; Cui, Y. Spinel $LiMn_2O_4$ Nanorods as Lithium Ion Battery Cathodes. *Nano Lett.* **2008**, *8*, 3948−3952.

(5) Amatucci, G. G.; Pereira, N.; Zheng, T.; Tarascon, J. M. Failure Mechanism and Improvement of the Elevated Temperature Cycling of $LiMn_2O_4$ Compounds through the Use of the $LiAl_xMn_{2-x}O_{4-z}F_z$ Solid Solution. *J. Electrochem. Soc.* **2001**, *148*, A171−A182.

(6) Amine, K.; Liu, J.; Kang, S.; Belharouak, I.; Hyung, Y.; Vissers, D.; Henriksen, G. Improved Lithium Manganese Oxide Spinel/Graphite Li-Ion Cells for High-Power Applications. *J. Power Sources* **2004**, *129*, 14−19.

(7) Hammami, A.; Raymond, N.; Armand, M. Runaway Risk of Forming Toxic Compounds. *Nature* **2003**, *424*, 635−636.

(8) Amine, K.; Liu, J.; Belharouak, I. High-Temperature Storage and Cycling of C-$LiFePO_4$/Graphite Li-Ion Cells. *Electrochem. Commun.* **2005**, *7*, 669−673.

(9) Zhou, S.; Han, H.; Nie, J.; Armand, M.; Zhou, Z.; Huang, X. Improving the High-Temperature Resilience of $LiMn_2O_4$ based Batteries: LiFNFSI an Effective Salt. *J. Electrochem. Soc.* **2012**, *159*, A1158−A1164.

(10) Sun, Y. K.; Hong, K. J.; Prakash, J.; Amine, K. Electrochemical Performance of Nano-sized ZnO-Coated $LiNi_{0.5}Mn_{1.5}O_4$ Spinel as 5 V Materials at Elevated Temperatures. *Electrochem. Commun.* **2002**, *4*, 344−348.

(11) Guan, D.; Jeevarajan, J. A.; Wang, Y. Enhanced Cycleability of $LiMn_2O_4$ Cathodes by Atomic Layer Deposition of Nanosized-Thin Al_2O_3 Coatings. *Nanoscale* **2011**, *3*, 1465−1469.

(12) Li, B.; Wang, Y.; Rong, H.; Wang, Y.; Liu, J.; Xing, L.; Xu, M.; Li, W. A Novel Electrolyte with the Ability to form a Solid Electrolyte Interface on the Anode and Cathode of a $LiMn_2O_4$/Graphite Battery. *J. Mater. Chem. A* **2013**, *1*, 12954.

(13) Ryou, M.-H.; Hong, S.; Winter, M.; Lee, H.; Choi, J. W. Improved Cycle Lives of $LiMn_2O_4$ Cathodes in Lithium Ion Batteries by an Alginate Biopolymer from Seaweed. *J. Mater. Chem. A* **2013**, *1*, 15224.

(14) Wang, X.; Liu, Z.; Kong, Q.; Jiang, W.; Yao, J.; Zhang, C.; Cui, G. A Single-Ion Gel Polymer Electrolyte Based on Polymeric Lithium Tartaric Acid Borate and Its Superior Battery Performance. *Solid State Ionics* **2014**, *262*, 747−753.

(15) Qin, B.; Liu, Z.; Ding, G.; Duan, Y.; Zhang, C.; Cui, G. A Single-Ion Gel Polymer Electrolyte System for Improving Cycle Performance of $LiMn_2O_4$ Battery at Elevated Temperatures. *Electrochim. Acta* **2014**, *141*, 167−172.

(16) Zhang, J.; Yue, L.; Hu, P.; Liu, Z.; Qin, B.; Zhang, B.; Wang, Q.; Ding, G.; Zhang, C.; Zhou, X.; Yao, J.; Cui, G.; Chen, L. Taichi-Inspired Rigid-Flexible Coupling Cellulose-Supported Solid Polymer Electrolyte for High-Performance Lithium Batteries. *Sci. Rep.* **2014**, *4*, 6272−6272.

(17) Zhu, Y.; Xiao, S.; Shi, Y.; Yang, Y.; Wu, Y. A Trilayer Poly(vinylidene fluoride)/Polyborate/Poly(vinylidene fluoride) Gel Polymer Electrolyte with Good Performance for Lithium Ion Batteries. *J. Mater. Chem. A* **2013**, *1*, 7790.

(18) Ahmad, A.; Isa, K. B. M.; Osman, Z. Conductivity and Structural Studies of Plasticized Polyacrylonitrile (PAN) - Lithium Triflate Polymer Electrolyte Films. *Sains Malays.* **2011**, *40*, 691−694.

(19) Rajendran, S.; Babu, R.; Sivakumar, P. Optimization of PVC−PAN-based Polymer Electrolytes. *J. Appl. Polym. Sci.* **2009**, *113*, 1651−1656.

(20) Flora, X. H.; Ulaganathan, M.; Rajendran, S. Role of Different Plasticizers in Li-Ion Conducting Poly(acrylonitrile)-Poly(methyl methacrylate) Hybrid Polymer Electrolyte. *Int. J. Polym. Mater.* **2013**, *62*, 737−742.

(21) Zhang, J.; Liu, Z.; Kong, Q.; Zhang, C.; Pang, S.; Yue, L.; Wang, X.; Yao, J.; Cui, G. Renewable and Superior Thermal-Resistant Cellulose-based Composite Nonwoven as Lithium-Ion Battery Separator. *ACS Appl. Mater. Interfaces* **2013**, *5*, 128−134.

(22) Zhuang, Q.; We, i. T.; Du, L.; Fang, L.; Sun, S. An Electrochemical Impedance Spectroscopic Study of the Electronic and Ionic Transport Properties of Spinel $LiMn_2O_4$. *J. Phys. Chem. C* **2010**, *114*, 8614−8621.

(23) Wang, S. H.; Hou, S. S.; Kuo, P. L.; Teng, H. Poly(ethylene oxide)-co-Poly(propylene oxide)-based Gel Electrolyte with High Ionic Conductivity and Mechanical Integrity for Lithium-Ion Batteries. *ACS Appl. Mater. Interfaces* **2013**, *5*, 8477−8485.

(24) Pieczonka, N. P. W.; Yang, L.; Balogh, M. P.; Powell, B. R.; Chemelewski, K.; Manthiram, A.; Krachkovskiy, S. A.; Goward, G. R.; Liu, M.; Kim, J.-H. Impact of Lithium Bis(oxalate)borate Electrolyte Additive on the Performance of High-Voltage Spinel/Graphite Li-Ion Batteries. *J. Phys. Chem. C* **2013**, *117*, 22603−22612.

DOI: 10.1021/am5083683
ACS Appl. Mater. Interfaces 2015, 7, 4720−4727

(25) Aurbach, D.; Levi, M. D.; Levi, E.; Teller, H.; Markovsky, B.; Salitra, G.; Heider, U.; Heider, L. Common Electroanalytical Behavior of Li Intercalation Processes into Graphite and Transition Metal Oxides. *J. Electrochem. Soc.* **1998**, *145*, 3024−3034.
(26) Aurbach, D.; Levi, M. D.; Gamulski, K.; Markovsky, B.; Salitra, G.; Levi, E.; Heider, U.; Heider, L.; Oesten, R. Capacity Fading of $Li_xMn_2O_4$ Spinel Electrodes Studied by XRD and Electroanalytical Techniques. *J. Power Sources* **1999**, *81*, 472−479.
(27) Amatucci, G. G.; Schmutz, C. N.; Blyr, A.; Sigala, C.; Gozdz, A. S.; Larcher, D.; Tarascon, J. M. Materials' Effects on the Elevated and Room Temperature Performance of $C/LiMn_2O_4$ Li-Ion Batteries. *J. Power Sources* **1997**, *69*, 11−25.
(28) Dedryvere, R.; Laruelle, S.; Grugeon, S.; Gireaud, L.; Tarascon, J. M.; Gonbeau, D. XPS Identification of the Organic and Inorganic Components of the Electrode/Electrolyte Interface Formed on a Metallic Cathode. *J. Electrochem. Soc.* **2005**, *152*, A689−A696.
(29) Jang, D. H.; Oh, S. M. Electrolyte Effects on Spinel Dissolution and Cathodic Capacity Losses in 4 V $Li/Li_xMn_2O_4$ Rechargeable Cells. *J. Electrochem. Soc.* **1997**, *144*, 3342−3348.
(30) Gummow, R. J.; Dekock, A.; Thackeray, M. M. Improved Capacity Retention in Rechargeable 4 V Lithium Lithium Manganese Oxide (Spinel) Cells. *Solid State Ionics* **1994**, *69*, 59−67.
(31) Tsunekawa, H.; Tanimoto, S.; Marubayashi, R.; Fujita, M.; Kifune, K.; Sano, M. Capacity Fading of Graphite Electrodes Due to the Deposition of Manganese Ions on Them in Li-ion Batteries. *J. Electrochem. Soc.* **2002**, *149*, A1326−A1331.
(32) Gnanaraj, J. S.; Pol, V. G.; Gedanken, A.; Aurbach, D. Improving the High-Temperature Performance of $LiMn_2O_4$ Spinel Electrodes by Coating the Active Mass with MgO via a Sonochemical Method. *Electrochem. Commun.* **2003**, *5*, 940−945.
(33) Cho, J. P.; Kim, T. J.; Park, B. The Effect of a Metal-Oxide Coating on the Cycling Behavior at 55 Degrees in Orthorhombic $LiMnO_2$ Cathode Materials. *J. Electrochem. Soc.* **2002**, *149*, A288−A292.
(34) Aurbach, D.; Gamolsky, K.; Markovsky, B.; Gofer, Y.; Schmidt, M.; Heider, U. On the Use of Vinylene Carbonate (VC) Electrolyte Solutions for Li-Ion as an Additive to Batteries. *Electrochim. Acta* **2002**, *47*, 1423−1439.
(35) Zhan, C.; Lu, J.; Kropf, A. J.; Wu, T.; Jansen, A. N.; Sun, Y.-K.; Qiu, X.; Amine, K. Mn(II) Deposition on Anodes and Its Effects on Capacity Fade in Spinel Lithium Manganate-Carbon Systems. *Nat. Commun.* **2013**, *4*, 2437.

DOI: 10.1021/am5083683
ACS Appl. Mater. Interfaces 2015, 7, 4720−4727